Available online at www.sciencedirect.com
SCIENCE DIRECT®
Optical Fiber Technology 12 (2006) 10–19
Optical Fiber Technology
www.elsevier.com/locate/yofte

Temperature-dependent fluorescence characteristics of an ytterbium-sensitized erbium-doped silica fiber for sensor applications

Seungin Baek [a,*], Yoonchan Jeong [b], Johan Nilsson [b], Jayanta K. Sahu [b], Byoungho Lee [a]

[a] *School of Electrical Engineering, Seoul National University, Kwanak-Gu Shinlim-Dong, Seoul 151-744, Republic of Korea*

[b] *Optoelectronics Research Centre, University of Southampton, Southampton SO17 1BJ, United Kingdom*

Received 30 November 2004; revised 12 April 2005

Available online 13 May 2005

Abstract

The characteristics of temperature-dependent fluorescence of an ytterbium (Yb^{3+})-sensitized erbium (Er^{3+})-doped silica fiber are presented. A 10-cm long double-clad Yb^{3+}/Er^{3+}-codoped fiber is diode-pumped at 915 nm and the individual fluorescence intensities from Yb^{3+} and Er^{3+} ions are measured with varying the fiber temperature. The ratio of the dual fluorescence intensities varies exponentially with temperature in the range of room temperature to ~300 °C. This dual-dopant system has dual emission bands that emit comparable fluorescence powers. Particularly, the self-referencing fluorescence intensity ratio is insensitive to external perturbations in the fiber, which is useful for sensors that are used in a harsh environment without any use of additional referencing techniques. This scheme allows a compact, long-life, and low-cost temperature sensor and can also be combined with a wide range of existing fiber-optic multiplexing schemes that can simultaneously detect multiple physical parameters.

Keywords: Fiber-optic sensor; Yb^{3+}-sensitized Er^{3+}-doped fiber; Fluorescence; Intensity-based method

* Corresponding author. Fax: +82 2 873 9953.
E-mail address: cherub0@snu.ac.kr (S. Baek).

1068-5200/$ – see front matter
doi:10.1016/j.yofte.2005.04.002

1. Introduction

Optical fiber sensors have widely been used to detect various physical parameters, for example, temperature, strain, bending, stress, chemicals, etc. [1–7]. Among them, the silica-based fiber-optic sensors for efficient temperature detection have been studied as a basic but important topic in this field because they allow nearly instant response as well as giving very high precision. Furthermore, they can be implemented in a distributed sensor network [8–10]. A variety of temperature measurement methods via optical fibers include Bragg gratings [8], scattering [9,10], or fluorescence-based techniques [11–13]. Fiber Bragg gratings are very efficient at temperature sensing and are easy to implement; however, they always need additional techniques to discriminate the Bragg shifts by temperature and by strain/compression [3,8]. On the contrary, the fluorescence-based techniques are relatively independent of ambient conditions besides temperature. One of the widely used methods is the detection of fluorescence lifetimes [12–14]. This method can be utilized with various rare-earth-doped silica fibers. In principle, fluorescence is induced by pump power at a certain wavelength that is suitable for the doped ions, and a straightforward detection procedure is simply needed. Additional advantage of such rare-earth-doped fiber sensors is that they are compatible with a wide range of existing fiber-optic multiplexing schemes that can simultaneously detect multiple physical parameters [3,4].

Here, we present the characteristics of temperature-dependent fluorescence of a 10-cm long double-clad, Yb^{3+}-sensitized Er^{3+}-doped silica fiber (YESF). The dual dopants of Yb^{3+} and Er^{3+} ions generate fluorescence-power amounts in different rates with temperature when they are diode-pumped, and the ratio between them varies with temperature. This property is based on the fact that the energy transfer rate between Yb^{3+} and Er^{3+} ions is thermally coupled because the population densities of the ions are dependent on temperature. Even when a strong perturbation is involved in the fiber, the fluorescence intensity ratio (FIR) is likely to be kept valid [11], which suggests that this scheme would be useful for sensor applications that need self-referencing or those used in a harsh environment. This scheme can also be combined simultaneously with a wide range of existing fiber-optic multiplexing schemes.

In the following, we present a simplified theoretical background regarding the temperature characteristics of Yb^{3+}/Er^{3+}-codoped systems, experiments and implementation together with a simulation result, and concluding remarks.

2. Theory of temperature characteristics of Yb^{3+}/Er^{3+}-codoped system

When a rare-earth-doped system is pumped with a fixed rate, the fluorescence variation including a lifetime change can reflect the corresponding temperature [12]. Based on this property, various rare-earth ions, such as Er^{3+}, Yb^{3+}, Nd^{3+}, etc., have been investigated for fiber-optic sensors [13–15].

In fact the emission is proportional to the population of each energy level, and hence, the ratio of the fluorescence intensity from two thermally coupled energy levels can be

described by [11,16]

$$\frac{N_2}{N_1} = \frac{I_{2j}}{I_{1j}} = \frac{g_2\sigma_{2j}\omega_{2j}}{g_1\sigma_{1j}\omega_{1j}} \exp\left(\frac{-\Delta E}{kT}\right) = B\exp\left(\frac{-\Delta E}{kT}\right), \tag{1}$$

where N_i, I_{ij}, g_i, σ_{ij}, and ω_{ij} are the number of ions, fluorescence intensity, degeneracy, the emission cross section, and the angular frequency of fluorescence transmission from the upper ($i = 2$) and lower ($i = 1$) thermalizing energy levels to the terminal level j, respectively. ΔE is the energy difference between the two thermally linked levels, k is the Boltzmann constant, and T is the temperature in Kelvin. In practice several effects, for example, the overlap of fluorescence peaks originating from the two individual thermally coupled energy levels, have been shown to cause a deviation of the measured FIR from the behavior predicted by the Boltzmann distribution of Eq. (1). Thus, Eq. (1) can be modified into the following equation:

$$\text{FIR} = \left(\frac{n_2}{n_1}\right) B\exp\left(\frac{-\Delta E}{kT}\right) + \left(\frac{m_1}{n_1}\right), \tag{2}$$

where n_i defines the fraction of the total fluorescence intensity of the transition originating from level i actually measured by the detector for the i level and m_i defines the fraction of the total intensity from level i which is measured by the detector for the other thermalizing level [11].

Temperature-dependent changes in the intensity of the fluorescence usually arise due to the temperature dependence of nonradiative transition rates of the energy level or, in some circumstances, of the population of other energy levels of the doped ions. Therefore, by measuring the fluorescence intensity originating from a particular level, the temperature could in principle be inferred. Although fluorescence changes can be directly translated into the corresponding temperature, the simple intensity-based detection scheme, obviously, cannot resolve out any additional perturbations in the fiber or transmission losses of the fiber. One way to resolve this drawback is to detect fluorescence intensities at two different energy levels (wavelengths) that have different temperature dependencies if the intermediate loss, which can be introduced by bending loss, transmission loss, and pump loss with the fiber, is nearly identical for the emissions at different wavelengths (see Eq. (1)) [11]. In addition, the emission lines should be sufficiently separated; otherwise the sensitivity can be too low to obtain reasonable accuracy because the resultant ΔE becomes small (see Eq. (2)). Although we can choose two different energy levels that a single dopant can introduce, in general one emission band is dominant that the others are likely to become too small to detect. On the other hand, if a dual-dopant system is considered, there is a good possibility to have dual emission bands which emit comparable fluorescence powers. Here, a dual-dopant system of a YESF is investigated. Although the upconversion luminescence intensity ratio $^2H_{11/2}/^4S_{3/2}$ in Yb^{3+}/Er^{3+}-codoped bulk fluoride phosphate glasses was investigated with different temperature conditions showing a good linearity with temperature [17], the upconversion fluorescence is not perfect for sensor applications because of the extremely low efficiency of the process.

On the contrary, a YESF has strong emissions both at ~1 and at ~1.5 μm that are more suitable for senor applications. The energy level diagram of Yb^{3+}/Er^{3+} ions in a silica fiber is shown in Fig. 1. The absorption of pump photons by Yb^{3+} ions promotes electrons

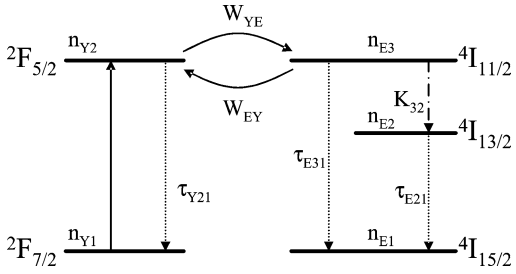

Fig. 1. Schematic diagram of the energy levels of Yb^{3+} and Er^{3+} ions in a YESF. Forward and backward energy transfer mechanisms are indicated while the upconversion of the Er^{3+} ions is neglected.

from the ground state $^2F_{7/2}$ to the $^2F_{5/2}$ manifold, which is followed by the energy transfer from $^2F_{5/2}$ level to the $^4I_{11/2}$ level of Er^{3+} ions and the nonradiative decay to the $^4I_{13/2}$ level. If the pump power is sufficiently low, the upconversion absorption of Er^{3+} ions does not significantly change the dynamics of the $^4I_{11/2}$ level of Er^{3+} ions and the $^2F_{5/2}$ level of Yb^{3+} ions. The rate equations for this process can be expressed as follows [18]:

$$\frac{\mathrm{d}n_{\mathrm{Y2}}}{\mathrm{d}t} = W_{\mathrm{EY}} n_{\mathrm{Y1}} n_{\mathrm{E3}} - W_{\mathrm{YE}} n_{\mathrm{Y2}} n_{\mathrm{E1}} - \frac{n_{\mathrm{Y2}}}{\tau_{\mathrm{Y21}}}$$
$$= -\left(K_{\mathrm{YE}} + \frac{1}{\tau_{\mathrm{Y21}}} \right) n_{\mathrm{Y2}} + K_{\mathrm{EY}} n_{\mathrm{E3}}, \tag{3}$$

$$n_{\mathrm{Y1}} = N_{\mathrm{Yb}} - n_{\mathrm{Y2}}, \tag{4}$$

$$\frac{\mathrm{d}n_{\mathrm{E3}}}{\mathrm{d}t} = W_{\mathrm{YE}} n_{\mathrm{Y2}} n_{\mathrm{E1}} - W_{\mathrm{EY}} n_{\mathrm{Y1}} n_{\mathrm{E3}} - K_{32} n_{\mathrm{E3}} - \frac{n_{\mathrm{E3}}}{\tau_{\mathrm{E31}}}$$
$$= -\left(K_{\mathrm{EY}} + \frac{1}{\tau_{\mathrm{E3}}} \right) n_{\mathrm{E3}} + K_{\mathrm{YE}} n_{\mathrm{Y2}}, \tag{5}$$

$$\frac{\mathrm{d}n_{\mathrm{E2}}}{\mathrm{d}t} = K_{32} n_{\mathrm{E3}} - \frac{n_{\mathrm{E2}}}{\tau_{\mathrm{E21}}}, \tag{6}$$

$$n_{\mathrm{E1}} = N_{\mathrm{Er}} - n_{\mathrm{E3}} - n_{\mathrm{E2}}, \tag{7}$$

where $1/\tau_{\mathrm{E3}} = 1/\tau_{\mathrm{E31}} + K_{32}$. $n_{\mathrm{Y}i}$ and $n_{\mathrm{E}i}$ are the population densities of Yb^{3+} and Er^{3+} ions at level i, respectively. N_{Yb} and N_{Er} are the total dopant concentrations of the Yb^{3+} and Er^{3+} ions. W_{YE} and W_{EY} are the cross-relaxation coefficients, which are the macroscopic energy transfer parameters of an Er^{3+}/Yb^{3+}-codoped system. These describe forward ($Yb^{3+} \rightarrow Er^{3+}$) and backward ($Er^{3+} \rightarrow Yb^{3+}$) energy transfer processes, respectively. K_{YE} and K_{EY} are the forward and backward energy transfer rates, respectively. In the equilibrium state between the forward and the backward energy transfer process with $K_{\mathrm{YE}} n_{\mathrm{Y2}} = K_{\mathrm{EY}} n_{\mathrm{E3}}$, the ratio of the energy transfer rates are described as [18]

$$\frac{K_{\mathrm{YE}}}{K_{\mathrm{EY}}} = \frac{n_{\mathrm{E3}}}{n_{\mathrm{Y2}}} = \frac{N_{\mathrm{Er}} g_{\mathrm{E3}}}{N_{\mathrm{Yb}} g_{\mathrm{Y2}}} \exp\left(\frac{-\Delta E}{kT} \right). \tag{8}$$

The population density of each state is related to temperature because the corresponding lifetime of each state is dependent on temperature. As a result, the energy transfer rate that is a function of the population density can indicate the temperature of the system. Therefore

the FIR between the emissions at ∼1 and ∼1.5 μm in a YESF can be a key to determining temperature that is nearly independent of other physical parameters. Considering the ratio of the energy transfer rates (Eq. (8)), the FIR (Eq. (2)) can be modified into the following equation:

$$\mathrm{FIR}' = B_1' + B_2' \exp\left(\frac{-\Delta E'}{kT}\right), \tag{9}$$

where B_j' ($j = 1$ or 2) and $\Delta E'$ are the modified factors that are accompanied by the concentration-dependent energy transfer rates between the $^2F_{5/2}$ level of the Yb^{3+} ion and the $^4I_{11/2}$ level of the Er^{3+} ion as well as the energy difference between the $^2F_{5/2}$ level of the Yb^{3+} ion and the $^4I_{13/2}$ level of the Er^{3+} ion. The characteristics of this measure are experimentally investigated in the following section in comparison with a numerical simulation.

3. Experiments

The experimental arrangement is shown in Fig. 2. A YESF was drawn from a preform that was fabricated in-house by the modified chemical-vapor-deposition (MCVD) and solution-doping technique. It had an Yb^{3+}/Er^{3+}-codoped core of a diameter of 9 μm and a numerical aperture (NA) of 0.16. The concentrations of Yb^{3+} and Er^{3+} ions are approximately 20,000 and 1000 ppm, respectively. The inner cladding was made of pure silica and had a diameter of 150 μm. It was coated by a low-index polymer outer cladding that provided an NA of 0.48. This double-clad structure allows the use of a multimode diode pump source for exciting the rare-earth ions. The thermal damage threshold of this polymer coating is approximately 150 °C, which is potentially the upper limit of the temperature that is allowed to the fiber. In order to increase the temperature range, all-glass fibers are preferred and can easily be implemented. However, in the experiment, the

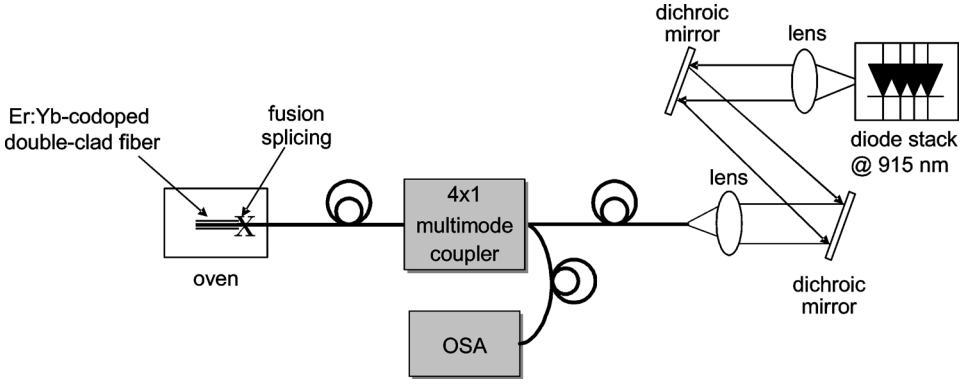

Fig. 2. Experimental setup for the measurement of temperature-dependent fluorescence characteristics of a YESF. The light from the pump source is launched into the 4 × 1 multimode coupler via lenses and dichroic mirrors. The backward fluorescence is detected by an optical spectrum analyzer.

polymer coating was simply striped off to eliminate the coating damage in higher temperature, i.e., the outer cladding was replaced with an air surround of which refractive index is ∼1. A 10-cm long fiber was used in the experiment. This length was simply determined to enable sufficient fluorescence power as well as adequate pump absorption. The YESF section was fusion-spliced to a standard multimode-fiber coupler and was kept in a temperature-controlled oven. A laser diode emitting at 915 nm was used to excite Er^{3+} ions via Yb^{3+} ions. In fact, the YESF has the main absorption peak at ∼975 nm and the second absorption peak at ∼915 nm. The peak absorption at ∼975 nm is typically more than five times larger than the absorption at ∼915 nm, whereas absorption band around ∼975 nm is more than three times narrower than that around ∼915 nm. In

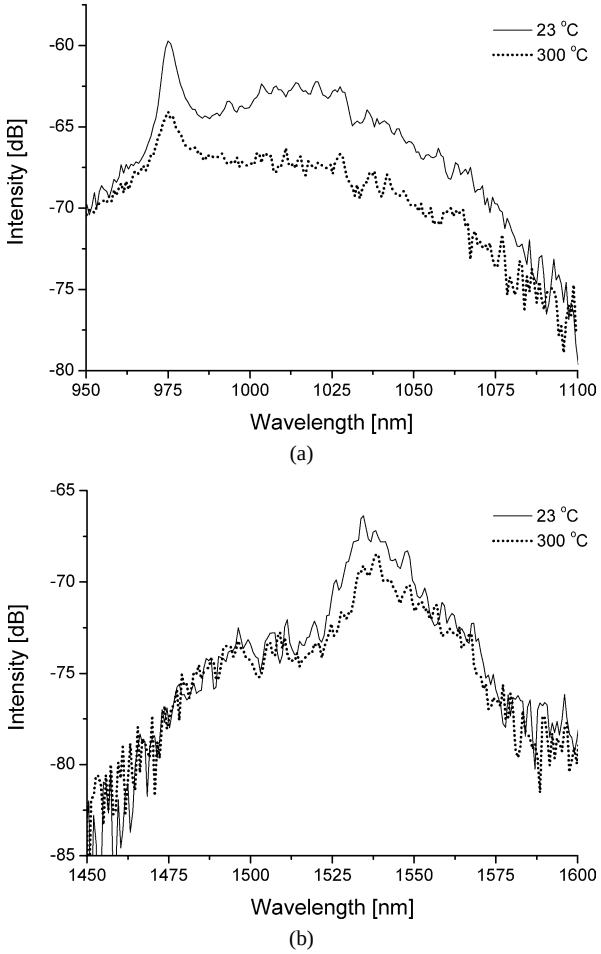

Fig. 3. Spectral fluorescence intensity profiles with respect to temperature from (a) Yb^{3+} and (b) Er^{3+} ions, respectively. It is seen that the fluorescence intensities from the codoped ions are in a comparable level and decrease with temperature.

addition, the center wavelength of a pump source is changed with pump current. Thus, the absorption when a 975-nm pump source is used is not always stronger than when a 915-nm one is used [19]. In the experiment, relatively small pump power that is enough to generate fluorescence and not to start lasing is needed. Therefore, a 915-nm pump source is appropriate. The pump light was coupled into the multimode-fiber coupler, and the backward-propagating fluorescence was detected by an optical spectrum analyzer. The nominal pump power measured in free-space between the two lenses (see Fig. 2) was $\sim$1 W and the coupling efficiency into the multimode-fiber coupler was 60%. When a pump source with single-mode pigtailed output and a 2×1 single-mode coupler are available, the pump power needed can be reduced and the system can be realized more cost-effectively.

Figures 3a and 3b show the individual emission spectra from Yb^{3+} and Er^{3+} ions, respectively, with respect to temperature. It can be seen that the fluorescence intensities from the codoped ions are in a comparable level and decrease with temperature. The fluorescence intensities at fixed wavelengths 1012.5 and 1537.5 nm are shown in Figs. 4a and 4b (resolution bandwidth: 2 nm), respectively. These wavelengths are the fluorescence lines from one of the manifolds of the $^2F_{5/2}$ level (Yb^{3+}) and the $^4I_{13/2}$ level (Er^{3+}) to the terminal levels of $^2F_{7/2}$ (Yb^{3+}) and $^4I_{15/2}$ (Er^{3+}), respectively. The squares in Fig. 4c represent the measured ratio of the intensities from Yb^{3+} and Er^{3+} ions, while the solid line represents the theoretical expectation based on Eq. (9). The simulation parameters are $B_1' = 1.35$, $B_2' = 0.011$, which were determined iteratively, and $\Delta E' = -1000.5\ \mathrm{cm}^{-1}$. Although the temperature characteristics of the YESF can be dependent on many factors, the theoretical estimation is in good agreement with the measurement. It is worth noting that even though the energy transfer rate between the $^2F_{5/2}$ level of the Yb^{3+} ion and the $^4I_{11/2}$ level of the Er^{3+} ion and the energy difference between the $^2F_{5/2}$ level of Yb^{3+}

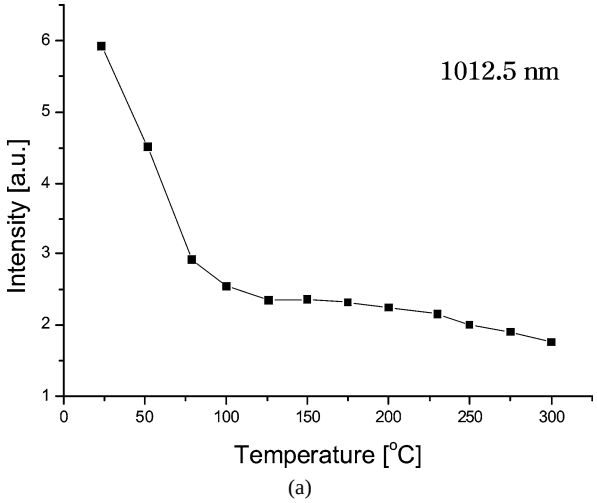

(a)

Fig. 4. Fluorescence intensities at fixed wavelengths with respect to temperature are shown (a) for Yb^{3+} (1012.5 nm) and (b) for Er^{3+} (1537.5 nm) ions, respectively. (c) The squares represent the measured data for the intensity ratio, and the solid line represents the theoretical estimation based on Eq. (9).

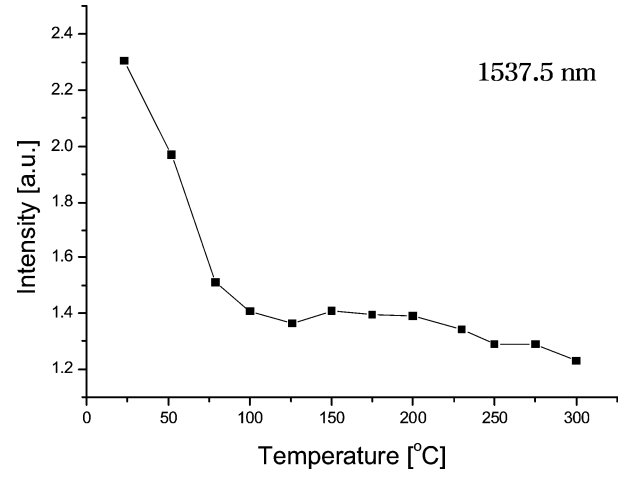

(b)

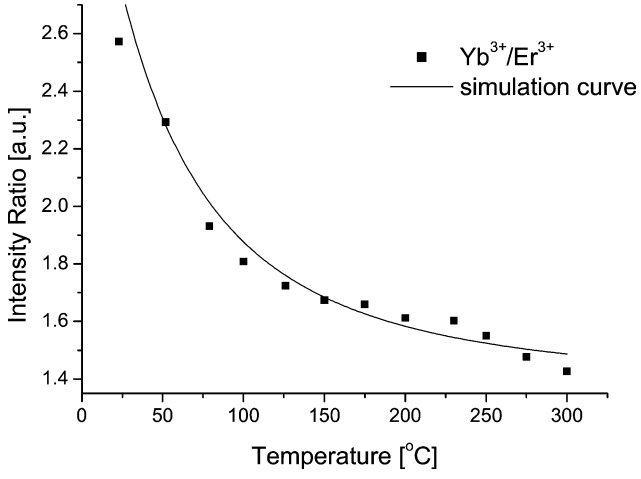

(c)

Fig. 4. (Continued.)

ions and the $^4I_{13/2}$ level of Er^{3+} ions are not explicitly separated, the approximation based on Eq. (9) is in good agreement. The negative sign to $\Delta E'$ in the exponent in Eq. (9) is due to the fact that the energy level of $^2F_{5/2}$ (Yb^{3+}) is higher than that of $^4I_{15/2}$ (Er^{3+}), which leads to an exponentially decaying form of the FIR variation with respect to temperature. It is noteworthy that even when strong perturbations are involved in the fiber, the FIR can be insensitive to them from the point of view of the effects induced by those external perturbations because they are nearly even to the two different emission lines, thereby being canceled out within the ratio. This suggests that the proposed scheme can be useful for sensor applications that need self-referencing or those used in a harsh environment.

4. Conclusion

We have characterized the temperature-dependent fluorescence of a 10-cm long YESF for potential sensor applications. The temperature range of room temperature to ~300 °C was investigated. The fluorescence spectra via both Yb^{3+} and Er^{3+} ions were measured and the mutual intensity ratio (FIR) was calculated. This FIR varies exponentially with temperature, thereby indicating the temperature. The temperature resolutions of the order of 1 °C in the low-temperature region ($T < 150$ °C) and of the order of 10 °C in the high-temperature one ($T > 150$ °C) were obtained. The resolution in the high-temperature region is somewhat low, however, that in the low-temperature one is compatible with other fluorescence-based temperature sensors [11–14]. Our numerical model of the FIR with respect to temperature was in good agreement with the experimental data. This 10-cm piece YESF can be used as a sensor head which allows a compact, long-life, and low-cost temperature sensor. This scheme can also be combined with a wide range of existing fiber-optic multiplexing schemes that can detect multiple physical parameters simultaneously.

References

[1] A.D. Kersey, M.A. Davis, H.J. Patrick, M. LeBlanc, K.P. Koo, C.G. Askins, M.A. Putnam, E.J. Friebele, Fiber grating sensors, J. Lightwave Technol. 15 (1997) 1442–1463.
[2] B. Lee, Review of the present status of optical fiber sensors, Opt. Fiber Technol. 9 (2003) 57–79.
[3] M. Song, S.B. Lee, S.S. Choi, B. Lee, Simultaneous measurement of temperature and strain using two fiber Bragg gratings embedded in a glass tube, Opt. Fiber Technol. 3 (1997) 194–196.
[4] K.J. Han, Y.W. Lee, J. Kwon, S. Roh, J. Jung, B. Lee, Simultaneous measurement of strain and temperature incorporating a long-period fiber grating inscribed on a polarization-maintaining fiber, IEEE Photon. Technol. Lett. 16 (2004) 2114–2116.
[5] F.J. Arregui, C. Fernandez-Valdivielso, I. Ilundain, I.R. Matias, A pH sensor made using cellulosic coating on a biconically tapered single-mode optical fiber, Proc. SPIE 4185 (2000) 464–467.
[6] S. Baek, Y. Jeong, B. Lee, Characteristics of short-period blazed fiber Bragg gratings for use as macrobending sensors, Appl. Opt. 41 (2002) 631–636.
[7] R. Gafsi, P. Lecoy, A. Malki, Stress optical fiber sensor using light coupling between two laterally fused multimode optical fibers, Appl. Opt. 37 (1998) 3417–3425.
[8] J. Jung, N. Park, B. Lee, Simultaneous measurement of strain and temperature by use of a single fiber Bragg grating written in an erbium:ytterbium-doped fiber, Appl. Opt. 39 (2000) 1118–1120.
[9] D. Liu, Y. Tang, D. Yu, C. Ke, D. Huang, Distributed fiber-optic temperature sensor based on Raman scattering of data fiber, Proc. SPIE 4020 (2000) 293–299.
[10] R. Rathod, R.D. Pechstedt, D.A. Jackson, D.J. Webb, Distributed temperature-change sensor based on Rayleigh backscattering in an optical fiber, Opt. Lett. 19 (1994) 593–595.
[11] S.A. Wade, S.F. Collins, G.W. Baxter, Fluorescence intensity ratio technique for optical fiber point temperature sensing, J. Appl. Phys. 94 (2003) 4743–4756.
[12] D.I. Forsyth, T. Sun, K.T.V. Grattan, S.A. Wade, S.F. Collins, Characteristics of doped optical fiber for fluorescence-based fiber optic temperature systems, Rev. Sci. Instrum. 74 (2003) 5212–5218.
[13] Z.Y. Zhang, K.T.V. Grattan, A.W. Palmer, B.T. Meggitt, T. Sun, Fluorescence decay-time characteristics of erbium-doped optical fiber at elevated temperatures, Rev. Sci. Instrum. 68 (1997) 2764–2766.
[14] T. Sun, Z.Y. Zhang, K.T.V. Grattan, Erbium/ytterbium fluorescence based fiber optic temperature sensor system, Rev. Sci. Instrum. 71 (2000) 4017–4022.
[15] F. Sidiroglou, S.A. Wade, N.M. Dragomir, G.W. Baxter, S.F. Collins, Effects of high-temperature heat treatment on Nd^{3+}-doped optical fibers for use in fluorescence intensity ratio based temperature sensing, Rev. Sci. Instrum. 74 (2003) 3524–3530.

[16] S.F. Collins, G.W. Baxter, S.A. Wade, T. Sun, K.T.V. Grattan, Z.Y. Zhang, A.W. Palmer, Comparison of fluorescence-based temperature sensor schemes: Theoretical analysis and experimental validation, J. Appl. Phys. 84 (1998) 4649–4654.
[17] J.F. Philipps, T. Töpfer, H. Ebendorff-Heidepriem, D. Ehrt, R. Sauerbrey, Spectroscopic and lasing properties of Er^{3+}:Yb^{3+}-doped fluoride phosphate glasses, J. Appl. Phys. 72 (2001) 399–405.
[18] Z. Meng, K. Nagamatsu, M. Higashihata, Y. Nakata, T. Okada, Y. Kubota, N. Nishimura, T. Teshima, S. Buddhudu, Energy transfer mechanism in Yb^{3+}:Er^{3+}-ZBLAN: macro- and micro-parameters, J. Luminescence 106 (2004) 187–194.
[19] J. Nilsson, S.-U. Alam, J.A. Alvarez-Chavez, P.W. Turner, W.A. Clarkson, A.B. Grudinin, High-power and tunable operation of erbium–ytterbium co-doped cladding-pumped fiber lasers, IEEE J. Quantum Electron. 39 (2003) 987–994.